

University of Colorado Boulder
Department of Computer Science

The Roles of Inertia and Stability in Power Systems

Samantha Molnar

February 2019

Abstract

Power systems today are undergoing extreme changes with the integration of renewable generation sources such as solar and wind. With these new technologies come new challenges. Traditional generation sources, such as coal and natural gas, provide inertial support, which helps maintain system stability when an outage occurs. However, solar and wind generation do not, on their own, provide this support, which potentially makes the system more vulnerable to failures. The effect on stability as power engineers introduce more renewables into the generation mix remains an open question. I start to address this question by studying system dynamics by changing two aspects of inertia: the *total* system inertia and the *structural distribution* of inertia. I show how both of these aspects of inertia are important to power system dynamics. Specifically, I measure the frequency dynamics of cascading failure simulations under various inertia scenarios.

Contents

Abstract	i
1 Introduction	1
2 Power Systems Background	4
2.1 Structure and Organization of Power Systems	4
2.2 Power Flow Equations	6
2.3 Power System Dynamics	11
2.3.1 Inertia	13
2.4 Power System Stability	16
2.4.1 Frequency and Rotor Angle Stability Metrics	18
2.5 Cascading Failures in Power Systems	20
3 Role of Power System Inertia in Cascade Events	25
3.1 Experimental Setup	27

3.2 Preliminary Results	29
4 Conclusion	39
Bibliography	40

List of Figures

1.1	Left: Projected growth of fuel types, based on current trends in the energy market. Right: Amount of greenhouse gas emissions by energy fuel type, based on projected electricity consumption. Figures from the Energy Information Administration 2018 Annual Energy Outlook [3].	2
2.1	The interconnections of North America. Although interconnections are connected, they can function individually from each other. Image from [28]. . .	5
2.2	Basic illustration of an electric generator with the mechanical and electromagnetic phenomena labeled. Based on figures in [37] and [41].	12
2.3	An example of a frequency deviation after a loss of generation, with relevant frequency measures labeled.	19
2.4	An example of a rotor angle time series with acceptable (black line), and unacceptable (red line) behavior.	20
3.1	Plot of the power system test cases for the proposed experiments. Generators are marked in green; all other buses are in red.	28

3.2 Set of outcomes that can occur after an initial failure. (I) No other failures occur and the network remains connected. (II) $N - 1$ contingency disconnects the network, but no other failures occur. (III) A cascade of failures occurs but the network remains connected. (IV) A cascade of failures occurs and the network disconnects. The sizes of the circles do not indicate the number of scenarios that belong in each category.	30
3.3 Frequency dynamics of the Illinois 200 bus test case for an outage that falls into category (I).	31
3.4 Average over all category (I) contingencies of the maximum RoCoF for the Illinois 200 bus test case. A darker line color indicates a larger magnitude. . .	32
3.5 Frequency dynamics for each category (I) contingency as a function of inertia for the Illinois 200 bus test case. For clarity, a darker line indicates a larger value at 1% of the total system inertia.	32
3.6 Impact of inertia distance on frequency deviations for category (I) contingencies of the Illinois network. The colored points in the left plot correspond to the colored edges in the right plot.	33
3.7 Frequency dynamics for the category (III)	35
3.8 Category (II) time series and frequency dynamics.	36
3.9 Category (IV) time series and frequency dynamics.	37

Chapter 1

Introduction

Power systems today are undergoing significant changes in an effort to make them more sustainable and environmentally friendly. This is due to the fact that electricity is one of the largest contributors to greenhouse gases in the U.S., only slightly below transportation [14]. Until very recently, the majority of these emissions were due to the significant use of coal as a fuel source for electricity, as seen on the right side of Figure 1.1. However, based on the lowering price of natural gas and variable renewable generation (VRG), such as wind and solar photovoltaics (PV), it is expected that VRG will contribute at least as much energy as coal by the year 2050¹ (see left panel of Figure 1.1) [3].

These forecasts indicate a need to understand how VRG will reshape power-system operations. Power systems function based on a delicate balance between the generation and consumption of electricity. This balance must be maintained at all time scales, from seconds to days and everything in between. Managing this balance is well understood when the generation sources have a controllable fuel source, such as coal or natural gas. But these well-established procedures have been disrupted by VRG; renewable resources are not controllable in the same ways as traditional fuel sources. Specifically conventional generation

¹Note: These projections do not consider the Clean Power Plan implemented in 2014.

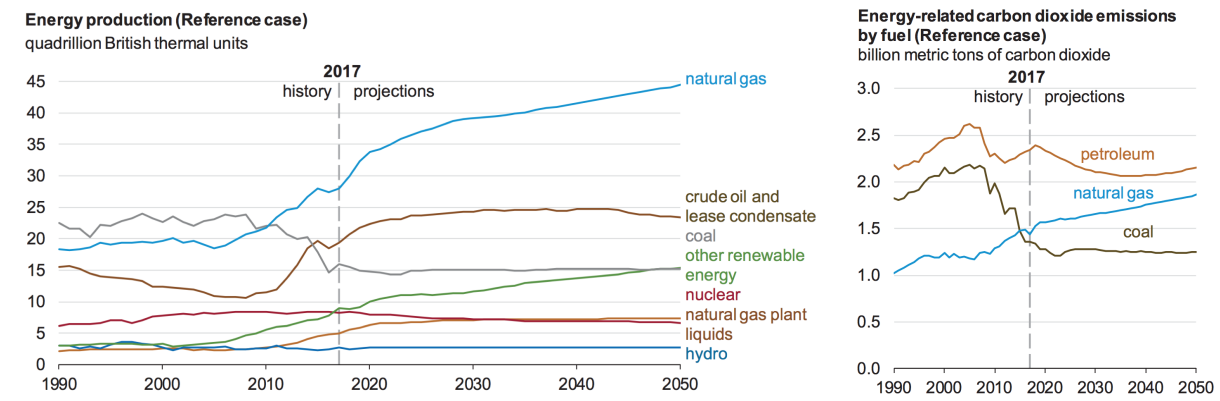


Figure 1.1: **Left:** Projected growth of fuel types, based on current trends in the energy market. **Right:** Amount of greenhouse gas emissions by energy fuel type, based on projected electricity consumption. Figures from the Energy Information Administration 2018 Annual Energy Outlook [3].

sources, such as gas or coal, are dispatchable, meaning the power output is controllable. On the other hand, wind and solar resources are determined by weather patterns, and thus uncontrollable. This issue means there need to be more grid flexibility options to compensate for this lack of control. Over the past decade, innovative solutions have emerged: storage technologies allow us to use solar power at night; aggregation of wind turbines helps smooth the intermittency of wind power. Cost incentives and increases in grid flexibility help explain rapid VRG adoption across the world. For example, in 2017 the Texas power system had large amount of wind generation. Wind energy production surpassed nuclear that year, at one point reaching a 54% instantaneous penetration [30].

As VRG replaces more thermal generation sources, new questions arise regarding grid stability. Traditional generators create electricity using large spinning rotors. When a power imbalance occurs, generators spin faster or slower to restore balance. This immediate response is determined by the *inertia* of each generator. However, VRGs do not have this spinning support, or inertia. Thus, as VRG levels increase, the natural balancing forces provided by and for traditional generators will decrease. It is this decrease in *inertial support* that has become a prominent issue in the power systems community, and on which I will focus.

The goal of this work is to characterize how inertia impacts system responsiveness to imbalances of electric power. As a first step, I test how system stability changes based on the *total* inertia and the *structural distribution* of inertia. I show that a decrease in total inertia has a non-linear impact on power system stability. Furthermore, I hypothesize that the location of low-inertia generators in the network has a strong influence on which perturbations create severe instabilities. These questions and results are discussed further in Chapter 3. The next chapter discusses the necessary terminology and mathematical foundations for that discussion.

Chapter 2

Power Systems Background

This chapter provides background regarding the terminology and modeling of power systems. Each section only provides an introduction to the topic which are whole areas of research on their own. The chapter begins with a discussion of the terminology and organizational structure of the U.S. power system, followed by modeling foundations. The final section describes cascading failures and a detailed description of the failure model used to study inertia in power system dynamics.

2.1 Structure and Organization of Power Systems

The basic components of power systems highlight key differences in its organization and structure. A power system consists of a generator and a load, with power lines connecting the two. Generators create electricity, while loads consume it. Based on distinct physical properties, the power systems community generally divides power lines into two networks: the transmission system and the distribution system. The transmission system is a mesh network that consists of high voltage power lines exchanging and delivering power over large regions. The distribution system tends to be a tree-like network which delivers power

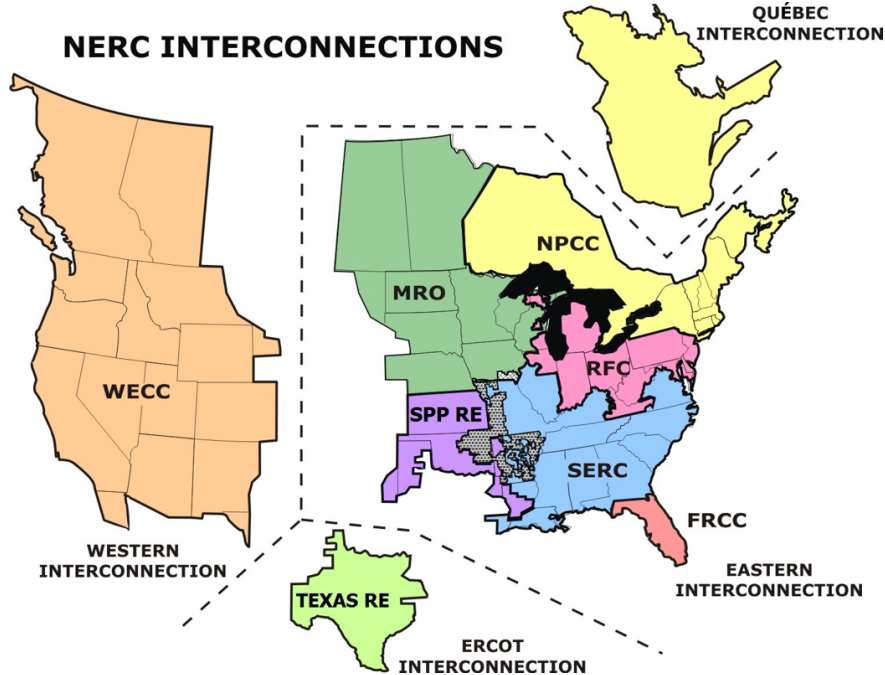


Figure 2.1: The interconnections of North America. Although interconnections are connected, they can function individually from each other. Image from [28].

from the transmission system to consumers. This work focuses on transmission systems because that's where the majority of traditional generation is being displaced by renewable generation. and add any shortcomings to this.

There are numerous entities involved in the control, regulation, and operation of transmission systems. In North America, there are two agencies that regulate power systems: the Federal Energy Regulatory Commission and the North American Electric Reliability Corporation. As the name may suggest, the Federal Energy Regulatory Commission (FERC) oversees energy markets, interstate energy exchanges, and quality standards [8]. The North American Electric Reliability Commission (NERC) creates and enforces statutes to ensure FERC standards are met [27]. NERC oversees four interconnections in the United States, as indicated by the dotted lines in Figure 2.1. In a given interconnection, all electric utilities are tied together, such that the stability of one depends on all the others. While each interconnection may exchange electricity, they can all function as individual power systems. Within each interconnection exist regional entities that carry out NERC standards. These

regional entities consist of multiple transmission system operators, generation providers, and distribution systems.

The organizations outlined in this section have a responsibility to define, study, and test the models and equations relevant to the secure operation of power systems. Often, the amount of mathematical detail varies based on the task at hand. For example, utility companies decide which generators to turn using the power flow equations. On the other hand, interconnections evaluate generation expansion plans based on system transient dynamics. This work requires both modeling details to accurately assess the impact of inertia on power systems. Thus, the rest of this chapter focuses on these mathematical descriptions.

2.2 Power Flow Equations

Power system modeling and analysis begins with a definition of how power flows from the generators to the loads. The power flow equations (PFE) describe how electricity travels through the network given the consumption and generation [6]. Specifically, the PFE solve for the current on every line and the voltage at every node. There are two types of electrical current: alternating current (AC) and direct current (DC). As power systems began to grow in size, there were debates over which was best to use¹. The debate involved efficiency and cost. It is more efficient to send power at a high voltage because it decreases the power lost through transmission lines. While high voltages *can* be achieved using DC, lowering the voltage to a safe level for consumers is still cheaper using an AC voltage transformer [41]. Thus, utility companies built transmission systems with AC power lines. As a consequence, power system modeling and analysis can be quite technical and intimidating. This section starts from a basic understanding of circuits and builds to the AC power flow equations (ACPFE).

¹ “Debates” is perhaps putting it lightly; it is more commonly referred to as the War of the Currents. I highly recommend *Empires of Light* by Jill Jonnes for more information.

The PFE describe physical quantities for buses (nodes) and lines (edges). There are three types of buses: generators, loads, and intermediaries. In this work, the set N of all buses has a cardinality of $|N| = n_b$. Generator buses are represented by the set G with cardinality $|G| = n_g$, and load buses by the set D with cardinality $|D| = n_d$. It is common practice in the power systems community to only represent generator and load buses, and this work adheres to that standard [12]. Finally, two buses i and j are connected if there exists a line l in the set of lines L . There are $|L| = n_l$ lines in the network. Most of this chapter identifies a line by the subscript ij , but the l subscript will become useful later on in the chapter.

Ohm's law defines the relationship between current (I), voltage (V), and resistance (R) for a simple DC circuit (Equation 2.1a).

$$I = \frac{V}{R} \quad (2.1a)$$

When inductors are present, the AC form of Ohm's law applies (Equation 2.1b); hence voltage (\bar{V}), current (\bar{I}), and impedance (\bar{Z}) are complex quantities.

$$\bar{I} = \frac{\bar{V}}{\bar{Z}} \quad (2.1b)$$

Specifically, the complex voltage and current are phasors with magnitudes and angles (Equations 2.2).

$$\bar{I} = |I| (\cos(\theta) + \mathbf{j} \sin(\theta)) \quad (2.2a)$$

$$\bar{V} = |V| (\cos(\delta) + \mathbf{j} \sin(\delta)) \quad (2.2b)$$

The physical parameters of a transmission line are quantified by impedance, where the real part is the resistance (R), and the imaginary part is the reactance (X) of the line (Equation 2.3).

$$Z = R + \mathbf{j}X \quad (2.3)$$

Resistance quantifies the opposition to the flow of current, while reactance quantifies the

opposition to the *change* in current or voltage.

Up until now, Equations 2.1-2.3 defined quantities for a single circuit element. However, as previously stated, a transmission system is a network consisting of *multiple* circuit elements (*i.e.* buses and nodes), and so matrix notation is used to represent this system of equations. In this chapter, bold symbols are used to represent matrices.

Before going any further, it is more efficient to use the *admittance* of a line, rather than the impedance. This is because the impedance matrix is dense and thus more computationally expensive than the admittance matrix, which is sparse. Admittance is simply the inverse of impedance (Equation 2.4).

$$Y = \frac{1}{Z} = G - \mathbf{j}B \quad (2.4)$$

Similarly, the conductance G is the inverse of resistance, and the susceptance B is the negative inverse of reactance.

Using the admittance substitution and matrix notation, Equation 2.1b is rewritten in Equation 2.5.

$$\mathbf{I} = \mathbf{Y}\mathbf{V} \quad (2.5)$$

Then, the current at bus i is the sum of the currents of all lines connected to that bus.

$$I_i = \sum_{j=1}^{n_b} Y_{ij} V_i$$

This is an exact statement of Kirchoff's current law, which falls out nicely from the matrix notation.

Finally, the last equation necessary to derive the PFE relates power to current and voltage.

This relationship is defined in Equation 2.6, where $*$ denotes a complex conjugate.

$$I_i = \sum_{j=1}^{n_b} Y_{ij} V_j = \frac{S_i^*}{V_i^*} \quad (2.6)$$

Complex power S_i has a real component and an imaginary component, as shown in Equation 2.7.

$$S_i^* = P_i + \mathbf{j}Q_i \quad (2.7)$$

The component P_i is the *real power*, and the imaginary component Q_i is the *reactive power*. Physically, real and reactive power are different types of energy used by different types of electrical components. Resistive components, such as light bulbs, consume real power while inductive components, such as air conditioners, consume both real and reactive power. There are also mathematical reasons for separating complex power into its real and imaginary parts, which will be explained later in this section.

The final step in the PFE derivation substitutes the phasor definition of voltage, Equation 2.2, into Equation 2.6. A helpful replacement is $\delta_{ij} = \delta_i - \delta_j$ for the difference in voltage angles between bus i and bus j .

$$S_i^* = P_i + \mathbf{j}Q_i = |V_i| \sum_{j=1}^{n_b} |V_j| (G_{ij} - \mathbf{j}B_{ij}) (\cos(\delta_{ij}) + \mathbf{j} \sin(\delta_{ij}))$$

This form easily separates the real and imaginary parts into two equations, shown below.

$$P_i = |V_i| \sum_{j=1}^{n_b} |V_j| (G_{ij} \cos(\delta_{ij}) + B_{ij} \sin(\delta_{ij})) \quad (2.8a)$$

$$Q_i = |V_i| \sum_{j=1}^{n_b} |V_j| (G_{ij} \sin(\delta_{ij}) - B_{ij} \cos(\delta_{ij})) \quad (2.8b)$$

Equations 2.8a - 2.8b describe the *alternating current power flow equations* (ACPFE). A

few parameters are given *a priori* to solve this system of equations. By convention, the real power ($P_i = P_g$), and voltage magnitude ($|V_i| = |V_g|$) of each generator is given, while the real power ($P_i = -P_d$) and reactive power ($Q_i = -Q_d$) is given for each load² [29]. Lastly, a reference node— the “slack” node— is defined for the system such that its voltage angle is always zero ($\delta_i = 0$). Generally, the slack node is chosen to be the largest generator [6].

The ACPFE can be difficult to solve in practice, for reasons discussed momentarily. Often, these equations are simplified for quick solutions, or for problems that require solving the PFE a large number of times [35]. This simplification is called the DC approximation, where “DC” means decoupled, **not direct current**. For this approximation, the following assumptions are made:

- $|\delta_{ij}|$ is small such that $\sin(\delta_{ij}) \approx \delta_{ij}$
- For every line, the resistance is much smaller than the reactance, which means $G_{ij} \approx 0$ and $B_{ij} \approx \frac{-1}{X_{ij}}$
- $|V_i| \approx 1, \quad \forall i \in N$
- $\forall i \in N Q_i$ is constant

The appropriate use of the DC approximation is a long-standing debate in the power systems community. Generally, the assumptions listed above are valid when the system is operating near a steady state [32]. When there are significant disturbances, though, there can be a discrepancy between the DC approximation and the ACPFE; solving the ACPFE in this situation is non-trivial [39]. Often, the solutions can diverge, which requires an exploration of multiple initial conditions to obtain convergence. Needless to say, a strict rule has not emerged from the community. The proposed research requires numerous simulations over a multitude of power system scenarios. The DC approximation is used in this work to keep computational times down.

²Note that the negative here means that real and reactive power are consumed at these nodes

The PFE solve for the equilibrium point, or steady-state, of a system. It is important to understand if a steady-state is a feasible solution given a number of physical constraints, such as line limits. While the PFE answer the question: “What are the equilibrium points of this system?”, power system dynamics answer questions such as: “How do state variables *behave* near the equilibrium point?” and “Will the system *evolve* back to a steady-state after a perturbation?” [41]. My research interests specifically involve the latter questions, which makes a background on power system dynamics necessary.

2.3 Power System Dynamics

Power system dynamics refers to the *dynamical* equations associated with the motion of the machines—generators and loads—in a system. In general, generator dynamics are consistent across dynamical models; usually, models are distinguished by the load dynamics [29]. I begin with a brief description of the physical phenomena occurring during power generation, followed by the equation of motion. This naturally flows into the equation of motion for loads. Generators produce electricity by converting *mechanical* energy into *electrical* energy [37]. The essential phenomenon that generators are utilizing is defined by Faraday’s law, which states that a changing magnetic field induces an electric field [CITE GRIFFITHS]. Figure 2.2 illustrates how this process is achieved. First, steam or falling water induces a torque on the turbine. The shaft of the turbine has a wire attached to it, which is in a magnetic field. When the turbine turns, so does the wire in the magnetic field, which causes a current to flow through the wire. The power a generator produces is exactly related to the speed at which the turbine rotates: the faster the turbine spins the more power it produces. The equation of motion for a generator relates the rotational speed and acceleration of the turbine to the power output. It is often referred to as the *swing equation*.

$$M_g \dot{\omega}_g + D_g \omega_g = P_{m_g} - P_{e_g}, \quad (2.9)$$

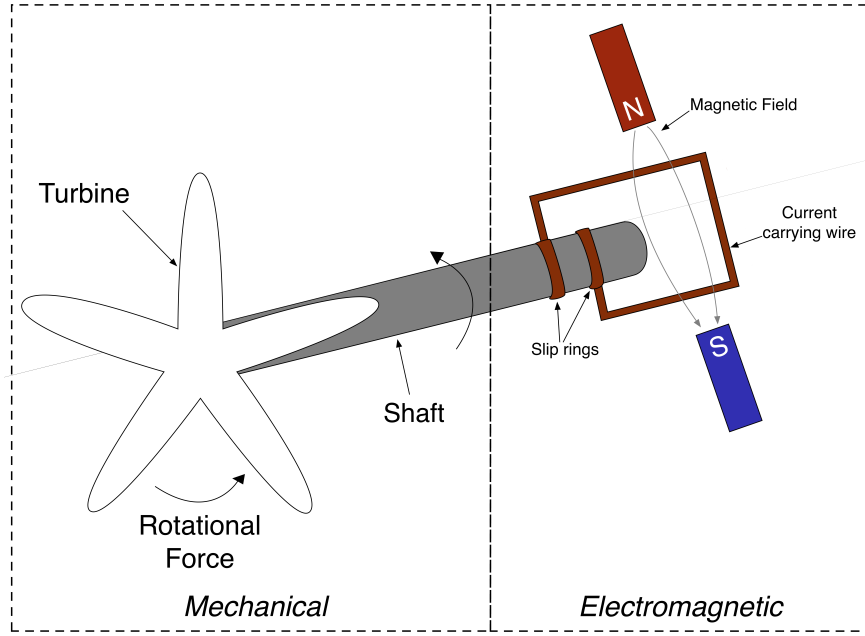


Figure 2.2: Basic illustration of an electric generator with the mechanical and electromagnetic phenomena labeled. Based on figures in [37] and [41].

$$\dot{\delta}_g = \omega_g - \omega_R, \quad \forall g \in G$$

Equation 2.9 is usually called the *swing equation* in the power-systems literature; it is a statement of Newton's second law. The constants M_g and D_g , the inertia and damping constants, are based on the type and mechanical specifications of the generator. The importance of the inertia constant is discussed in more detail in Section 2.3.1. The turbine angle, δ_g , and angular speed, ω_g , are defined with respect to a rotating reference frame ω_R (the slack bus). P_{m_g} is the mechanical power input to the machine's rotor, and P_{e_g} is the electric power output of the generator; thus $P_{m_g} - P_{e_g}$ describes how much energy is stored in the rotating armature of the generator [CITE].

Based on Equation 2.9, there are two variables that can change the speed of rotation of a generator. The first is by changing P_{m_g} , which is achieved by changing the amount of fuel that is burned. The second is by changing P_{e_g} which is achieved by a change in power consumption or flow in the network. The second point can be seen more clearly by substituting in the

power flow equations for P_{e_g} .

$$\dot{\omega}_g = -\frac{D_g}{M_g}\omega_g + \frac{1}{M_g}(P_g - \sum_{\forall i \notin G} b_{gi} \sin \delta_{gi}), \quad \forall g \in G \quad (2.10)$$

Interestingly, Equation 2.10 takes on the form of a second-order Kuramoto oscillator, which helped spark a broader interest in power system dynamics [1][4].

A key component of the structure preserving model is the representation of load nodes. Specifically, rather than modeling them as static variables, load nodes are also modeled as oscillators, but they are first order instead of second-order.

The load nodes is then modeled by Equation 2.11

$$\dot{\delta}_i = -\frac{1}{D_i}(P_i + \sum_{\forall j \in N} b_{ij} \sin \delta_{ij}), \quad \forall i \in L \quad (2.11)$$

where D_i is the damping term that describes the frequency dependence of the node.

More detailed descriptions of generator dynamics include the governor, which is responsible for controlling the generator frequency, and the excitation system, which controls the internal voltage magnitude of the generator. We do not consider these more detailed descriptions for the purposes of this work.

2.3.1 Inertia

We now take a moment to address the constant M_g introduced in Equation 2.10, which is of particular focus for this work. First, we will discuss what this constant means for thermal generators, such as coal or natural gas. We then outline how M_g changes for renewable generators, which leads us into stability considerations, which will be discussed in the next section.

Generation Type	Base Power Rating (MVA)	H (sec.)	M (MW · s)
Nuclear	1410 – 1504	3.8 – 4.24	5344 – 6530
Coal	194 – 1120	2.9 – 4.5	863 – 3158
Gas CT	7 – 235	1 – 12.5	22 – 1288
Gas Steam	14 – 887	1 – 5.4	13 – 2216
Gas CC	25 – 1433	1.1 – 9	97 – 8765
Hydro	10 – 70	2 – 3	19 – 1133

Table 2.1: Table of inertia values for various generation types in the ERCOT interconnection. Values obtained from [16].

A generator is a spinning rotor where the acceleration or deceleration determines its change in power output. The constant M_g is often referred to as the inertia constant, but it is perhaps better to refer to it as the inertia coefficient in this section. Often the inertia constant refers to the value H_g , which has units of seconds. H_g is based on the shape and size of the rotor, and it quantifies the amount of time a generator can provide its rated power S_g . These constants are all related based on Equation 2.12.

$$M_g = \frac{2S_g H_g}{\omega_R} \quad (2.12)$$

Based on this relation, M_g is really a description of the maximum amount of kinetic energy that could be stored in the rotor of a generator. Table 2.1 provides some typical values of the inertia constant H and the inertia coefficient M_g based on the generation type. These values are estimates for generators in the ERCOT interconnection, but it gives a sense of how the size of the turbine (which is related to the generation type) determines the inertia constant.

Lastly, it is often insightful to define the *total system inertia*. Often this is used when aggregating models for generators, but we will use it for a different purpose in Chapter 3. Equation 2.13 defines the total system inertia as a weighted sum of the inertia constant of every generator.

$$H_{tot} = \frac{\sum_{g=1}^{n_g} H_g S_g}{\sum_{g=1}^{n_g} S_g} \quad (2.13a)$$

$$M_{tot} = \sum_{g=1}^{n_g} M_g \quad (2.13b)$$

Unlike thermal generators, renewable generators must be connected to a transmission system through a power electronic device called an inverter. Typically multiple renewable generators, such as solar panels or wind turbines, are connected to one inverter. This simplifies control and increases power quality. Due to the fact that there are no spinning parts of an inverter, there is no natural inertia associated with renewable generation. In terms of the modeling equations, this simply means that $M_g = 0$, and the equation of motion for renewable generators then becomes equivalent to Equation 2.11 for loads³.

An important point to make about generator inertia is that it dictates the *immediate* response of a generator to a power imbalance. It describes the natural reaction of a generator to an increase or decrease in power consumption. However, due to the AC-DC inverter coupling, renewable generators do not have this natural reaction to power imbalances⁴. This fact can have important consequences on power system stability.

The next sections briefly introduce power system stability and cascading failures in power systems. Both of these phenomena have had multiple books and papers written on them; we do not try to cover these topics in their entirety. Instead, we introduce overall themes and important models or concepts relevant to the purposes of this work. Power system stability and cascading failures are highly interconnected phenomena; instabilities can precede cascades, or cascades can create instabilities. Although stability and cascades are highly

³Note that Equation 2.11 has the term P_i which is assumed to be negative for loads and positive for generators.

⁴Unless the inverter has special controls to create “virtual inertia”, which is a large research area we do not discuss in this work.

connected, a common research practice is to separate the study of the two. One reason for this is that each phenomenon is complicated enough to consider individually, let alone considering both. The following two sections outline power system stability and cascading failures. At the end of the chapter we introduce the model that will be used for the purposes of this work, which is a nice melding of stability and cascading failures.

2.4 Power System Stability

Broadly speaking, we define stability based on the ability of a dynamical system to return to an equilibrium state following a disturbance [20]. For power systems, there are three categories of stability found in the literature: voltage stability, frequency stability, and rotor angle stability. Each of these categories have a different driving force, even if they co-occur. We will outline the basic concepts of each category, but pay special attention to frequency and rotor angle stability, as these are most influenced by power system inertia.

Voltage stability is based on the system's ability to maintain bus voltages at an acceptable level. It is a measure of the balance between reactive power supply and demand [2]. One particular type of voltage instability that can lead to cascading failures is Fault-Induced Delayed Voltage Recovery. This occurs after a fault has been cleared in the system which leads to low voltages. These low voltages raise the reactive power requirement of motors, particularly air-conditioning units. When the reactive power cannot be met, the AC units stall, causing them to need 5-6 times the pre-contingency reactive power, this decreases the voltage further and can cause cascading failures [26]. In particular, this can cause voltage collapse, which is when the voltage of the nodes start to drop slowly and then quickly until the system cannot recover. Concerns about voltage instabilities have grown as more distributed solar has been added over the years. However, the focus of this work is on transmission systems, and in particular generator dynamics.

Frequency stability and rotor angle stability are dependent upon generator dynamics. Frequency stability is the ability of the system to maintain a frequency within a specified margin (60 ± 0.1 Hz in the U.S.) after an upset that causes an imbalance between real power generation and consumption. When generation is less than the load, there is a frequency drop, and vice versa when generation is greater than the load. If the frequency deviates too far from the nominal value equipment and/or load is disconnected to avoid damage. The severity of frequency excursions is discussed further in Section 2.4.1.

The frequency of a system is related to the inertia and rotor speed of each generator in an interconnection based on Equation 2.14. This is commonly referred to as the Center of Inertia (COI) frequency and is essentially a weighted average of the rotor speeds.

$$\omega_{COI} = \frac{\sum_{g=1}^{n_g} M_g \omega_g}{\sum_{g=1}^{n_g} M_g} \quad (2.14)$$

$$\omega = 2\pi f$$

Equation 2.14 is simple enough to compute for simulations; in practice, system frequency is usually measured at some relevant bus in the network even though this can be highly influenced by the generators that are closer to the bus.

Closely related to frequency stability is rotor angle stability, which is based on the individual oscillations of a generator. When a generator becomes out of sync with other generators due to an instability, usually the rebalancing forces from other generators will restore it to the proper oscillation speed and phase. This is dependent on the ability of the system to restore the equilibrium between the mechanical and electromagnetic torque of the generator. The system becomes unstable when it cannot absorb the kinetic energy caused from the differences in rotor speeds [19].

2.4.1 Frequency and Rotor Angle Stability Metrics

As we mentioned in Section 2.1, NERC creates and enforces minimum operating requirements for interconnections and balancing authorities. This section will define the relevant metrics for frequency and rotor angle stability.

There are a few metrics related to frequency stability. Consider for a moment a traditional power system with sufficient thermal generation, and small amounts of VRG penetration. After a loss of generation, the frequency of the system resembles Figure 2.3. There are three metrics we discuss here that quantify the severity of a frequency excursion. The first is the frequency NADIR, denoted by a blue point in Figure 2.3. This is the largest frequency deviation from the nominal frequency. Each interconnection has a specified Frequency NADIR where under-frequency load shedding (UFLS) occurs: eastern and western interconnections are 59.5 Hz, and ERCOT is 59.3 Hz. Related to the frequency NADIR is the rate of change of frequency (RoCoF), denoted by the green point in Figure 2.3. NERC analyzes the largest generation contingency that could occur in each interconnection and uses the RoCoF for these events to set limitation requirements. Internationally there are specific set points from as small as 0.5Hz/s in Ireland, to as high as 2.5Hz/s in Denmark [36]. Finally, the settling frequency, denoted by the dashed red line in Figure 2.3, is the settling frequency after a contingency occurs. This value indicates the effectiveness of generators to stabilize system frequency. When no generator controls are present, such as a governor, this value is usually determined by the damping capabilities of the remaining generators.

As we mentioned earlier in the text, rotor angle stability is closely related to frequency stability. Rotor angle stability is based on the damping capabilities of each individual generator, which in turn determines if it will remain synchronized with the system. NERC does not have a specific method of determining rotor angle stability, so we present the metric used by the Southwest Power Pool (SPP), a balancing authority in the Eastern interconnection [33].

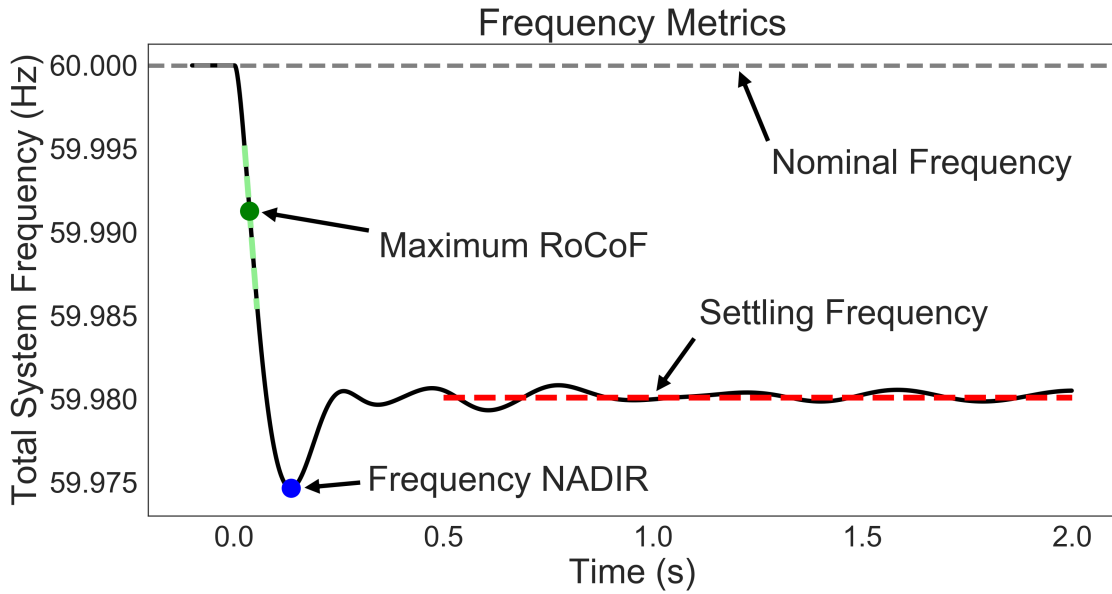


Figure 2.3: An example of a frequency deviation after a loss of generation, with relevant frequency measures labeled.

Figure 2.4 shows an example of two rotor angle time series; the black line has acceptable rotor angle stability while the red line has unacceptable rotor angle stability. Equation 2.15 defines the successive positive peak ratio, which uses the first and second positive peaks to quantify the damping of the generator.

$$SPPR = \frac{\text{Second Positive Peak} - \text{Minimum Value}}{\text{First Positive Peak} - \text{Minimum Value}} \leq 0.95 \quad (2.15)$$

In Figure 2.4, the first positive peak is denoted by a blue point, the second positive peak a green point, and the minimum value by a red point. The black line has $SPPR = 0.688$ which is considered to be a stable response.

The metrics discussed in this section will be used to evaluate the severity of cascading failures. We presented the measures that are most relevant when we consider power systems with changing inertia. The next section discusses the various ways cascading failures are modeled in the literature, and the model we choose to use for this work.

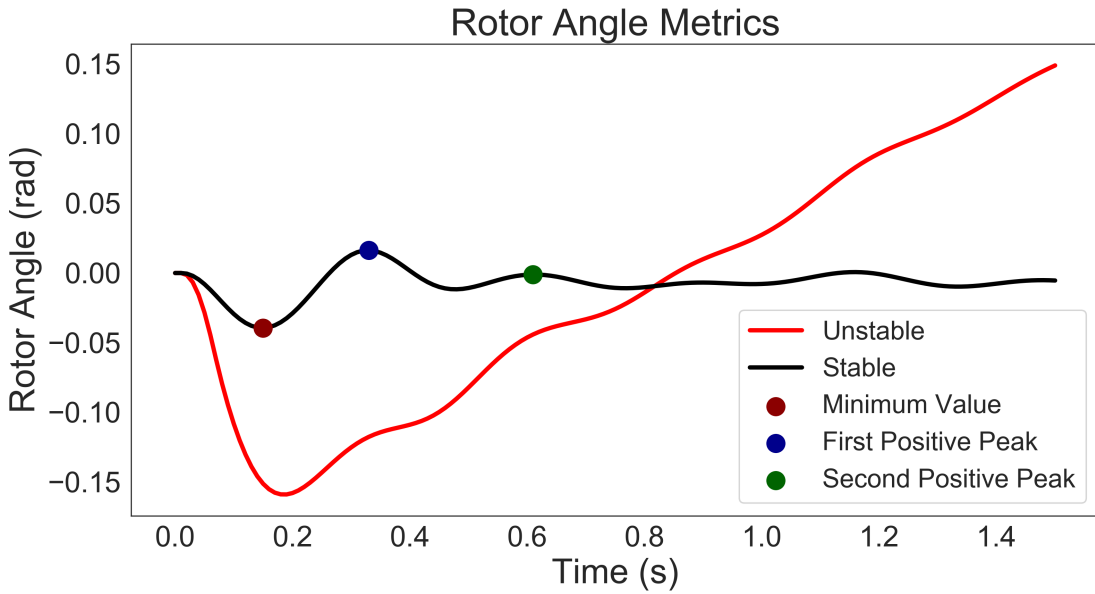


Figure 2.4: An example of a rotor angle time series with acceptable (black line), and unacceptable (red line) behavior.

2.5 Cascading Failures in Power Systems

Cascading failures are a ubiquitous phenomenon in many different types of networks. A cascade is dependent on the interaction of individual components and the topology of a network. When the component interactions are modeled linearly, such as in social networks, cascades evolve in a linear fashion. This means that when one component fails, the next component to fail will be connected to the failed component. This is not the case in power systems where cascades spread non-locally; when one component fails the next component failure is not necessarily adjacent. This is due to the non-linear nature of the power flow equations; in fact, there are no modeling assumptions in a linear cascade model that could accurately reflect the non-linearity of power system cascades [17]. As such, this section focuses on cascading failure models specific to power systems.

In power systems, cascading failures— colloquially referred to as blackouts— refers to the sequential loss of transmission lines. A cascade usually starts due to a random event, such as

untrimmed vegetation falling on a line [11]. When a line fails, this causes the power flow to be redistributed among the remaining lines. Each transmission line has a maximum capacity of power it can transport; when this limit is exceeded protection equipment stops the flow of current through the line. When power flow redistribution occurs, line flow limits might be exceeded, which causes another failure, and the power flow to again be redistributed; thus continuing the cascade. While a cascade is easy to describe, modeling its behavior can be quite tricky. Most cascading failure models differ by which power system dynamics are represented. We will focus on the difference between models that consider generator dynamics and those that do not.

A significant number of cascading failure models only implement the power flow equations outlined in Section 2.2. This is the simplest way to model cascades, while maintaining some sense of reality. The most prominent of these is the OPA model, which is named after the institutions of the original authors [10]. OPA is run over many “days”, where each day the following occurs: (I) the initial power flow of the system is solved, using the DC approximation, (II) an initial set of lines are removed at the beginning of the day based on a uniform probability, (III) power flow is re-solved with these lines removed, if any line is overloaded after resolving, it is removed with some probability. The cascade continues in this way until there are no longer overloaded lines. At the end of each “day” all lines that failed due to overload are upgraded, in that their capacity is increased, and the load that needs to be served is increased by some fraction. An important concept that followed from this model is that power systems are consistently operated at a critical level. OPA was the first model to introduce the idea that by running a power system in the most economical fashion (using all components at their maximum capacity, when necessary), also pushes it towards more critical regions. The OPA model captures the important characteristics of models that do not include generator dynamics. Similar models to OPA consider specific line failures, include generator re-dispatching, or add models of hidden failures of protection equipments [7, 15, 18]. The second type of cascade models also include generator dynamics, and this is

the model type we intend to use in this work.

Cascading failure models that consider generator dynamics— or transient stability— are less common in the literature. However, these models are perhaps the most important when we start to consider the effects of adding large amounts of renewable generation to power systems, specifically issues of inertia. Power flow based models do not describe these effects. We only discuss one cascading failure model that incorporates transient stability, but we note that there are a few others to keep in mind, such as [25] and [38].

The model we plan on using in this research is a continuous phase space (CPS) model that was first presented by [9] and then adapted and modified by [48]. The CPS model uses DC power flow equations and the generator swing Equation 2.10 and load Equation 2.11 for the transient dynamics. One major difference between the CPS model and other cascading failure models is the continuous nature of the line status. In most cascading failure models, the line status— call it η_{ij} — is a discrete variable. However, the CPS model treats it as a continuous variable and models it with a differential equation. This can be achieved in the following way. The overall goal is for the line status to evolve to $\eta_{ij} = 0$ when a line becomes overloaded. Let c_{ij} represent the fractional line capacity being used, such that $c_{ij} = 1$ means the line has the maximum amount of power flowing across it. Specifically, we define the limit of the line based on the maximum amount of charge that can flow through the line at any given time, or in other words, its maximum amount of energy. Thus, c_{ij} is just the integral of Equation 2.8a divided by the maximum amount of energy: $c_{ij} = \frac{B_{ij}(1-\cos\delta_{ij})}{W_{ij}}$.

In order to model the automatic removal of a line, the derivative of the line status should become negative as $c_{ij} \geq 1$. Based on the CPS model of [48], we use $\dot{\eta}_{ij} = f(\eta_{ij}) - c_{ij}$ where

$$f(\eta_{ij}) = \frac{1}{a} \left(\frac{1}{\eta_{ij}} - \frac{1}{1 - \eta_{ij}} \right) + a\eta_{ij}^4 - b$$

The quartic term ensures there are three roots of $f(\eta_{ij})$, and thus three equilibriums of $\dot{\eta}_{ij}$:

a stable equilibrium at $\eta_{ij} < 1$, a stable equilibrium at $\eta_{ij} \approx 0$, and an unstable equilibrium at $\eta_{ij} \approx 1$. In practice, $f(\eta_{ij})$ could be any function with the desired equilibria, in fact in [9] they use a sum of exponentials, but we will remain consistent with the model presented in [48] for this work. Although we discussed some of the necessary equations for the CPS model in Section 2.3, for completeness we reproduce all of them here.

$$\dot{\eta}_{ij} = 10(f(\eta_{ij}) - \frac{B_{ij}(1 - \cos \delta_{ij})}{W_{ij}}) \quad \forall i, j \in E \quad (2.16a)$$

$$\dot{\omega}_g = -\frac{D_g}{M_g}\omega_g - \frac{1}{M_g}(P_g + \sum_{\forall i \notin G} B_{gi} \sin \delta_{gi}) \quad \forall g \in G \quad (2.16b)$$

$$\dot{\delta}_g = \omega_g - \omega_1 \quad \forall g \in G \quad (2.16c)$$

$$\dot{\delta}_i = -\frac{1}{D_i}(P_i + \sum_{j=1}^{n_b} B_{ij}\eta_{ij} \sin \delta_{ij}) - \omega_1 \quad \forall i \notin G \quad (2.16d)$$

Although we have defined the line status as a continuous function in Equation 2.16a, it still essentially works as a boolean value which can be easily placed into the power flow and dynamical equations; in fact, Equation 2.11 and Equation 2.16d only differ by this term.

The CPS model as defined in [48] does not consider renewable generation sources, which is an essential component of this work. Similar to the approach taken in [42], we can modify the generator equation in the CPS model for a renewable source by setting $M_g = 0$. This change is shown in Equation 2.17, and has a similar form to the load equation 2.11. This equation is essentially like modeling a renewable source connected to a droop controller inverter, which is the simplest control mechanism in use. Equation 2.17 does not consider the power output of the generator P_{RG} to vary with time because the time scales we will be modeling are much smaller than measurement fidelity for most utility companies [21].

$$\dot{\delta}_{RG} = -\frac{1}{D_{RG}}(P_{RG} + \sum_{\forall i \notin G} B_{RG,i} \sin \delta_{RG,i}) - \omega_1 \quad (2.17)$$

Equations 2.16-2.17 represent the cascading failure model we will use in the proposed work.

The next chapter lays out the proposed work in detail.

Chapter 3

Role of Power System Inertia in Cascade Events

Power systems with high proportions of variable renewable generation (VRG), and therefore less inertia, have experienced increasing issues with stability and resiliency during cascades. For example, in 2016 a large blackout occurred in Australia where the entire southern region lost power. Preceding the blackout, wind generation was providing almost 50% of the power in that region when tornadoes disconnected multiple transmission lines. As a result, the interconnection lines between the north and the south overloaded and were tripped. The southern system did not have enough traditional synchronous generation (SG) available to stabilize the inevitable frequency deviations, which resulted in a frequency collapse [31].

The Southern Australia blackout underscores the need to understand the function of inertia during cascading failures. Specifically, two key aspects of inertia contributed to the blackout. First, high levels of renewable generation in the south meant low *total system inertia*. Second, the large-inertia SG (coal, natural gas) was easily separated from the low-inertia (wind); only a few transmission lines had to fail for the low-inertia generation to become isolated from the large-inertia generation. I will describe this issue as the *structural distribution of inertia*.

Both of these aspects of inertia—the overall amount and its location on the network—are crucial to system stability during cascading failures. The goal of this thesis is to gain a deeper understanding of the role of inertia in power system stability with a specific focus on the cascading failure dynamics of synthetic power systems.

Total system inertia has only been addressed by a few studies in limited contexts. Several investigations explored the effect of lower system inertia on system stability [13, 23, 24, 46], but exhaustive research on the relationship between system stability and total system inertia is notably absent from the literature. There is a documented need for this type of study; this past year, for instance, the Australian Energy Market Operator (AEMO) started requiring all power system operators to determine the level of system inertia needed to maintain system stability.

To address this gap, I will conduct an experiment that decreases total system inertia uniformly across the network—*i.e.*, reducing the inertia constant of every generator¹. The goal here is to study a simplified version of the problem that neglects the spatial distribution of inertia on the nodes of the network. This will allow for general conclusions to be drawn about the relationship between *total* system inertia and system stability.

The experiment proposed in the previous paragraph is not completely realistic, however; a better representation decreases inertia in a neighborhood of the network. This issue has only recently been recognized as a concern in the power-systems community [23]. Many studies about inertia placement in these systems have used unrealistically small test cases [40, 43]. Larger studies only focused on placement of control mechanisms, or only explored a few possible low-inertia scenarios [34, 47]. A study of a wide range of inertia distribution scenarios is needed because renewable generation is not added uniformly across the network. This is due to both resource availability and political incentives. The types of problems

¹Recall from Section 2.3, that total system inertia is the weighted sum of the inertia provided by every generator in the system (Equation 2.13)

that can arise from a poor placement of inertia are exemplified in the Southern Australian blackout.

The second part of the proposed work will explore this aspect of inertia. I will perform a wide range of possible inertia placement scenarios. Inertia values will be chosen based on representative values for given generation types (see Table 2.1). For this part of the study, I am specifically interested in how the separation between low and high inertia impacts stability. One way to quantify “separation” is by the average path length between generators with large and small inertia. I hypothesize that as the average path length between large and small inertia generation units increases, system instabilities during cascades will also increase. My placement scenarios will be chosen to explore this.

3.1 Experimental Setup

U.S. power grids are considered to be critical infrastructure. This means that information about the system—such as its structure and parameters—is exempt from public release. Therefore, it has become standard practice in the power systems community to experiment with synthetic networks that match the topology and dynamics of a power system *statistically*.

Following that approach, I will conduct the two proposed inertia alterations introduced above on two synthetic power network test cases. The first synthetic network is constructed using population and generation statistics for central Illinois with 200 nodes, 49 of which are generators; the second is based on the South Carolina power system with 500 nodes, 90 of which are generators. I will refer to these as the Illinois 200 bus test case and the South Carolina 500 bus test case, respectively. Both of these test cases are shown in Figure 3.1, with generators in green and all other buses in red.

Neither of these cases contain specific information about the actual power systems they

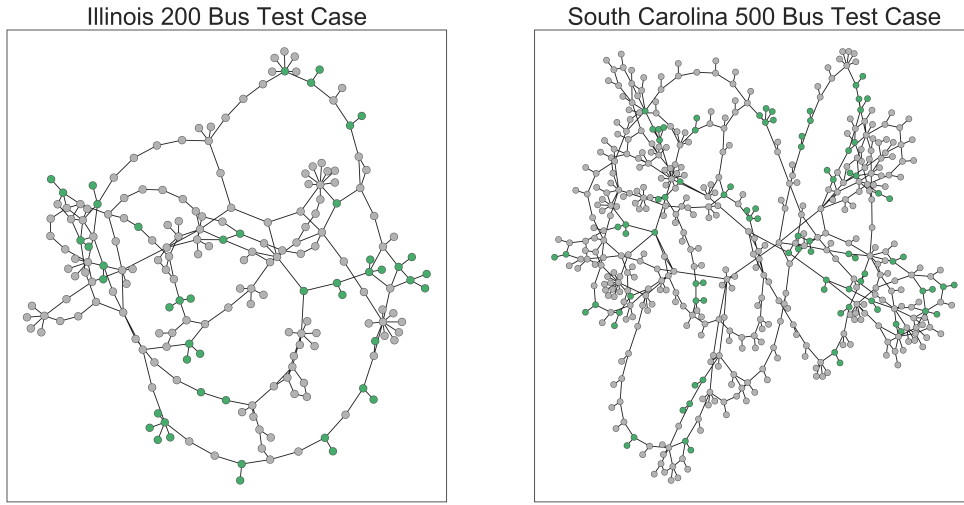


Figure 3.1: Plot of the power system test cases for the proposed experiments. Generators are marked in green; all other buses are in red.

represent. Rather, they were created using known information about the respective regions. Recall from Section 2.2, a basic requirement for any power systems study is the specification of the load and generation. For these test cases, the load information is based on the population data of that region and the generation type and size is based on data from the Energy Information Administration [5, 22]. Data about the generator dynamics, such as the inertia constants, are drawn from a distribution created from well-established test cases [45]. Finally, [44] applied a tuning procedure to the governor and stabilizer controls using common algorithms. The tuning was guided by standard stability metrics, some of which are outlined in Section 2.4.1.

For the purposes of this work, I made a few alterations to these test cases. First, [45] treat wind generators as having inertia. For realism, I will model all wind generators with no inertia. Second, solar generators are “netted” with the load. This means that the modeled power consumption is decreased by the total solar generation and the dynamics of these generators are not modeled. In this work, solar generator dynamics are modeled explicitly,

in a similar fashion as wind generators.

To study the effects of inertia on stability, I will run transmission line cascading failure simulations for the two sets of experiments listed above. Each cascade simulation generates a time series of the real power flow on each line, the voltage angle of every bus, and the rotor speed and angle of every generator. The specific cascading failure model is described in Section 2.5. Each simulation will be conducted in the following way. First, all parameters, including any inertia values, are initialized using data from [45] and the MATPOWER package [49]; then Equations 2.16 are solved using the Matlab `ode15s` solver for a time period of 20 seconds to ensure the system reaches a steady-state. (A time period of 20 seconds is approximately the amount of time that passes before generator control mechanisms turn on [37].) This will produce the baseline values for the system. Then I will trip k line(s) and re-run the simulation.

To quantify the severity of each cascade simulation, I will use a number of metrics on the total system frequency time series. Recall that the equation for total system frequency is a weighted average of the frequency of every generator (see Section 2.4). The two metrics of interest on the total system frequency time series are the maximum frequency deviation and the rate of change of frequency (RoCoF); both of these metrics are concerns as system inertia changes [23].

3.2 Preliminary Results

This section presents the results from the first experiment (reducing total system inertia) on the Illinois 200 bus test case. I refer to the scenario where no inertia changes are made as the “base total inertia”, or M_{tot} . Each change in total system inertia is given as a fraction or percentage of M_{tot} . The results of each cascade simulation are grouped into four categories according to the outcome of the simulation, as shown in Figure 3.2. Category (I) consists

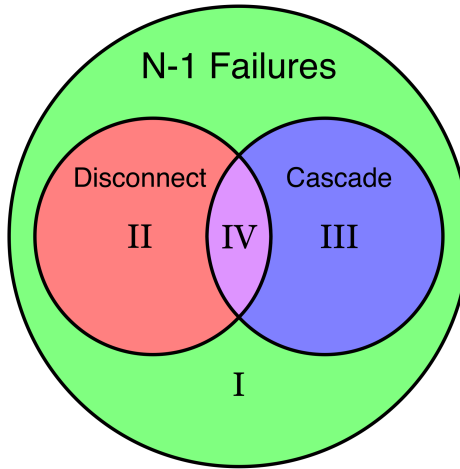


Figure 3.2: Set of outcomes that can occur after an initial failure. (I) No other failures occur and the network remains connected. (II) $N - 1$ contingency disconnects the network, but no other failures occur. (III) A cascade of failures occurs but the network remains connected. (IV) A cascade of failures occurs and the network disconnects. The sizes of the circles do not indicate the number of scenarios that belong in each category.

of the set of line contingencies that do not disconnect the network and do not result in a cascade. This is the largest category for the Illinois 200 bus system; of the 245 possible line failures, 171 of them fall into this category. Although this group of contingencies represents a class of failures with relatively stable dynamics, those dynamics are still important to understand. For instance, the European Network of Transmission System Operators (ENTSO) have indicated a need to quantify the RoCoF limits of system devices in terms of “normative” contingencies and future changes in system inertia [CITE]. Category (I) contingencies can be considered “normative” because the system returns to a steady-state without any other failures. Therefore, system limits should encompass all possible dynamics of category (I) contingencies, which requires a deeper understanding of those dynamics.

An example of the dynamical response to inertia changes for category (I) contingencies for the Illinois 200 bus test case is shown in Figure 3.3. Most prominently, as total inertia decreases the maximum frequency deviation increases. At the base total inertia the maximum

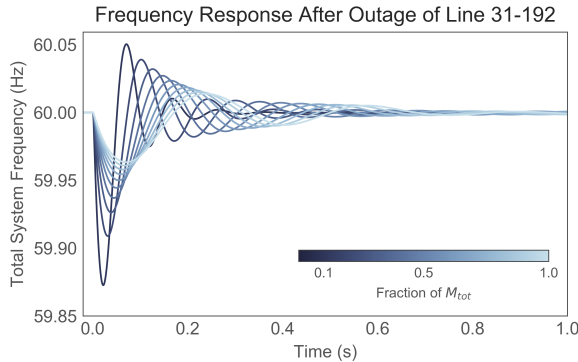


Figure 3.3: Frequency dynamics of the Illinois 200 bus test case for an outage that falls into category (I).

frequency deviation is approximately 0.01 Hz; this deviation increases to 0.2 Hz at 10% the base total inertia. Furthermore, the maximum deviation occurs at an earlier time as inertia decreases, which indicates an increasing RoCoF. Although a 90% reduction in inertia is not happening in the near future, it is informative to understand how the maximum frequency and RoCoF change as total system inertia decreases. To that end, Figures 3.4a and 3.4b show the maximum frequency deviation and RoCoF averaged over all category (I) contingencies. Clearly, both of these measures have a non-linear relationship with inertia. For each measure, I tried fitting different functions—exponentials, power law, *etc.*—to the data. The best fit, shown in blue, is of the form $a * x^{-b} + c$ for both the measures². The average maximum frequency deviation seems to scale as $\approx 1/M_{tot}^{0.15}$ and the RoCoF $\approx 1/M_{tot}^{0.73}$. This preliminary result quantifies the overall general trend of frequency and total system inertia. Other studies have generally found linear trends, perhaps because they have only explored a limited number of inertia values [46].

Of course, the averages shown in Figures 3.5a-3.5b are influenced by contingencies that cause larger deviations. Figure 3.5a shows the frequency deviation for each category (I) contingency. For clarity, contingencies with a larger value are shown with a darker color. Indeed, not all contingencies appear to grow in the same manner as the average shown in

²Furthermore, I took the logarithm of the total system inertia and each frequency measure and again solved for the best fit. This fit is linear, where the slope matches the exponent b shown here.

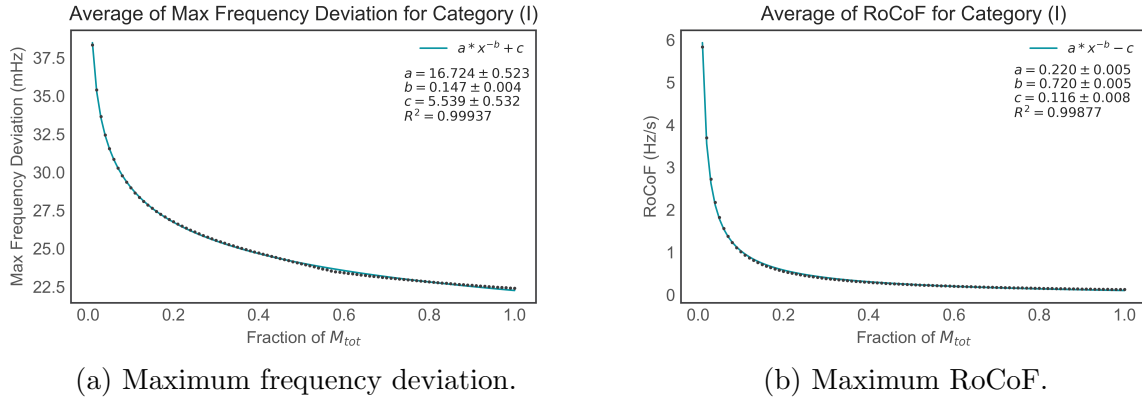


Figure 3.4: Average over all category (I) contingencies of the maximum RoCoF for the Illinois 200 bus test case. A darker line color indicates a larger magnitude.

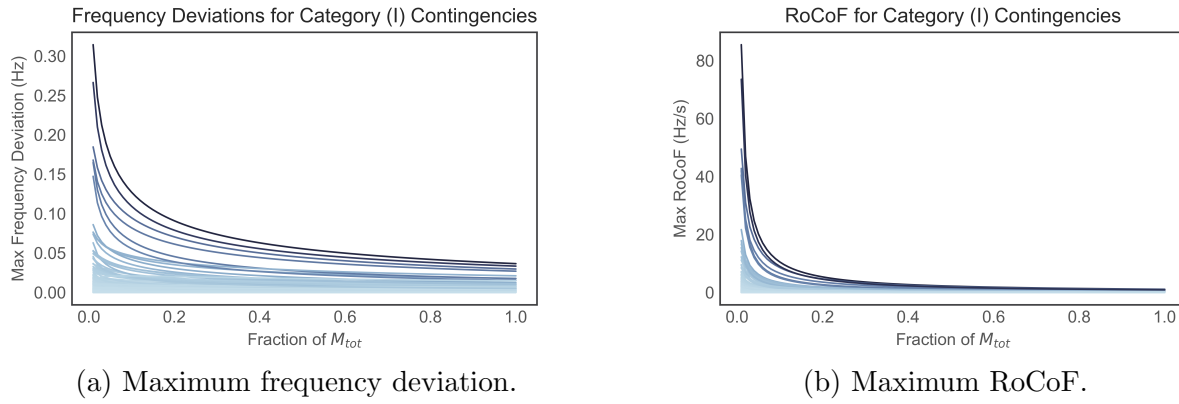


Figure 3.5: Frequency dynamics for each category (I) contingency as a function of inertia for the Illinois 200 bus test case. For clarity, a darker line indicates a larger value at 1% of the total system inertia.

Figure 3.4a. For example, the contingency shown in Figure 3.3 is the darkest line in Figure 3.5a, and has non-linear growth. However, it is also clear that if no deviation occurs at the base total system inertia, a decrease in inertia does not cause a deviation to occur (*i.e.* inertia is only important when a deviation occurs). Similarly, the RoCoF of each contingency is plotted in Figure 3.5b. The growth in RoCoF is more dramatic at low inertia values than the maximum frequency deviation. This makes sense because inertia specifically deals with a *change* in motion; less inertia means it is easier to move things faster. So far, all of these results have only investigated how the frequency dynamics change with total system inertia. As seen in Figures 3.5a and 3.5b, there is a wide range of possible frequency dynamics. This

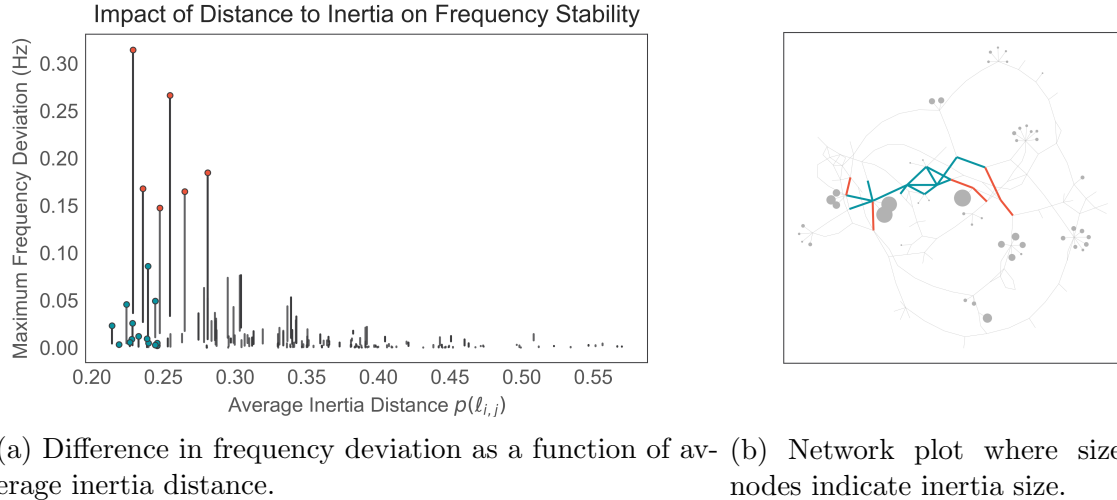


Figure 3.6: Impact of inertia distance on frequency deviations for category (I) contingencies of the Illinois network. The colored points in the left plot correspond to the colored edges in the right plot.

is likely due to the structure of the network, specifically the location of the contingency in relation to the generators. To better understand this, I introduce a new measure called the *average inertia distance* that quantifies the distance of a contingency to the inertia in the system, given by Equation 3.1.

$$p(\ell_{i,j}) = \frac{1}{M_{tot}} \sum_{g=1}^{n_g} M_g \frac{d(\ell_{i,j}, g)}{diam(G)} \quad (3.1)$$

Explicitly, let i and j be the buses that are connected by line $\ell_{i,j}$, the initially tripped line. I compute the minimum path length of each bus to a generator g and assign the minimum as the distance between the line and the generator $d(\ell_{i,j}, g) = \min[d(i, g), d(j, g)]$. I scale $d(\ell_{i,j}, g)$ by the longest shortest path in the network—the diameter of the network— $diam(G)$. I assign the weight $\frac{M_g}{M_{tot}}$ inertia to this distance.

Figure 3.6 shows the relationship between the average inertia distance and maximum frequency deviations. Figure 3.6a plots the change in the maximum frequency deviation from M_{tot} to $0.01M_{tot}$ for each contingency as a function of the average inertia distance. The length of the line indicates the change in the maximum frequency deviation, and the hori-

zontal location indicates the average inertia distance. Figure 3.6b plots the Illinois network with the size of the nodes indicating the amount of inertia provided by that node (so, only inertia providing generators have a non-zero size). The colored edges in Figure 3.6b correspond to the colored point in Figure 3.6a. In general, as the average inertia distance increases (*i.e.* contingencies are closer to larger-inertia generators) the maximum frequency deviation increases. For example, the red points in Figure 3.6a are indeed close to large inertia generation in Figure 3.6b. Most of them are only one link away from the large-inertia generation. However, there are some notable exceptions, marked with a blue point in Figure 3.6a and a blue edge in Figure 3.6b. First, these contingencies have as high or higher average inertia distance to the red points, but have a much lower frequency deviation. Based on Figure 3.6b the blue contingencies are not just close to one cluster of large inertia generation but are close to *multiple* large-inertia generation sources. This suggests that frequency deviations from multiple generation sources are cancelling each other out, sort of like an interference pattern.

The previous paragraph indicates two ideas. First, the distance to large-inertia generation is a general framework for determining the size of a frequency deviation. Specifically, the farther away a contingency occurs from large-inertia generation sources, the less impact it has on system frequency. Second, the closer to large-inertia sources, the more the network *topology* matters. Indeed, the blue edges in Figure 3.6b are part of triangles and cycles. They appear to be the “spine” of the network. A less dynamically stable outcome of a line contingency is one that results in a cascade, but does not disconnect the network: category (III) in Figure 3.2. The Illinois 200 bus test case only has one contingency that falls into this category. Figure 3.7a plots the time series for this contingency for various values of total system inertia and Figure 3.7b-3.7c show the frequency dynamics. The frequency dynamics follow a similar pattern to category (I) contingencies. This is because the network remains connected, which means that the coupling between all of the dynamic components does not change dramatically, as it does when a node becomes disconnected. As such, categories (I)

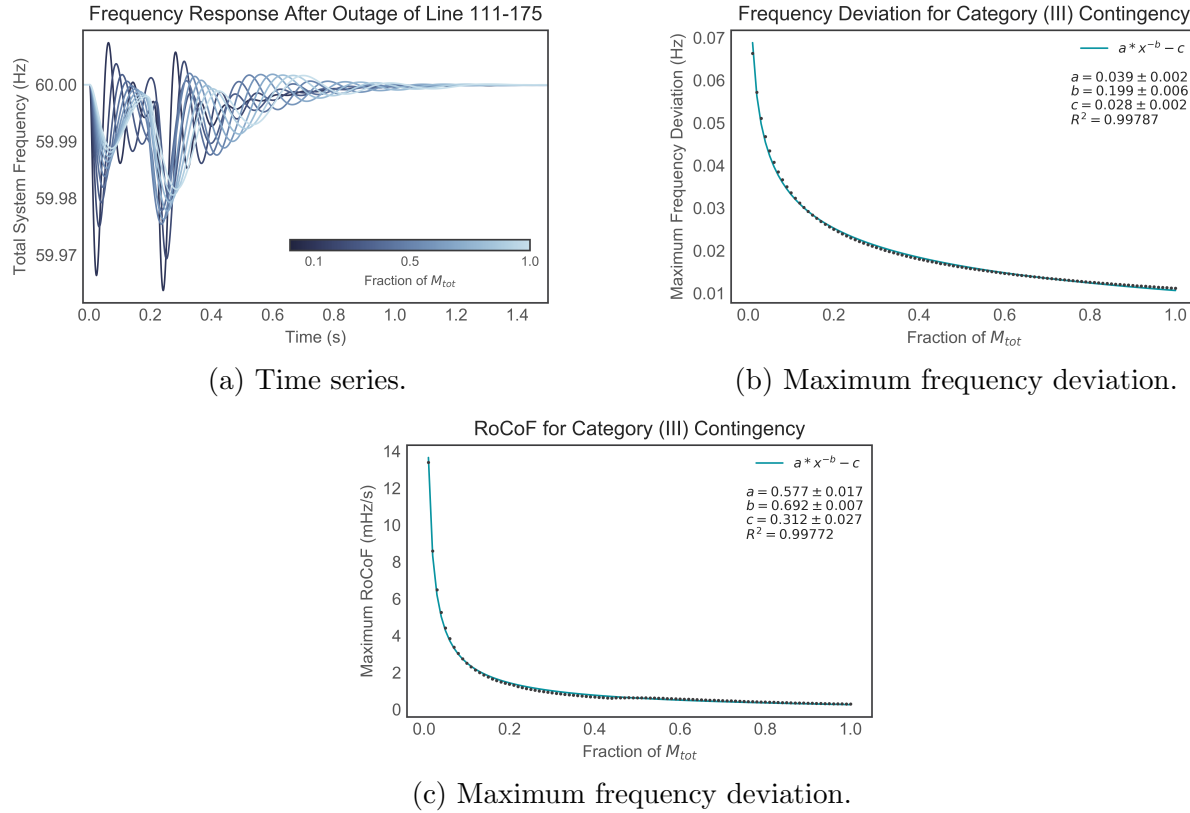


Figure 3.7: Frequency dynamics for the category (III)

and (III) can be considered dynamically similar.

Finally, the last two categories are the least dynamically stable as they result in a disconnected network. There are two ways this can happen: either the original contingency disconnected the network or the original contingency caused a cascade which then split the network. These are categories (II) and (IV) in Figure 3.2, respectively.

I consider two types of category (II) contingencies, one that disconnects a load bus, and one that disconnects a generator. The former is usually studied as a remedial action, while the latter is studied as an initiating event. Recall from Section 2.4 that frequency and rotor angle stability involve the study of system dynamics after the loss of generation (or load). Here, I focus on generators by convention. Recall from earlier in the chapter that the Illinois test case has VRG already added to the system. As such studying the removal of these

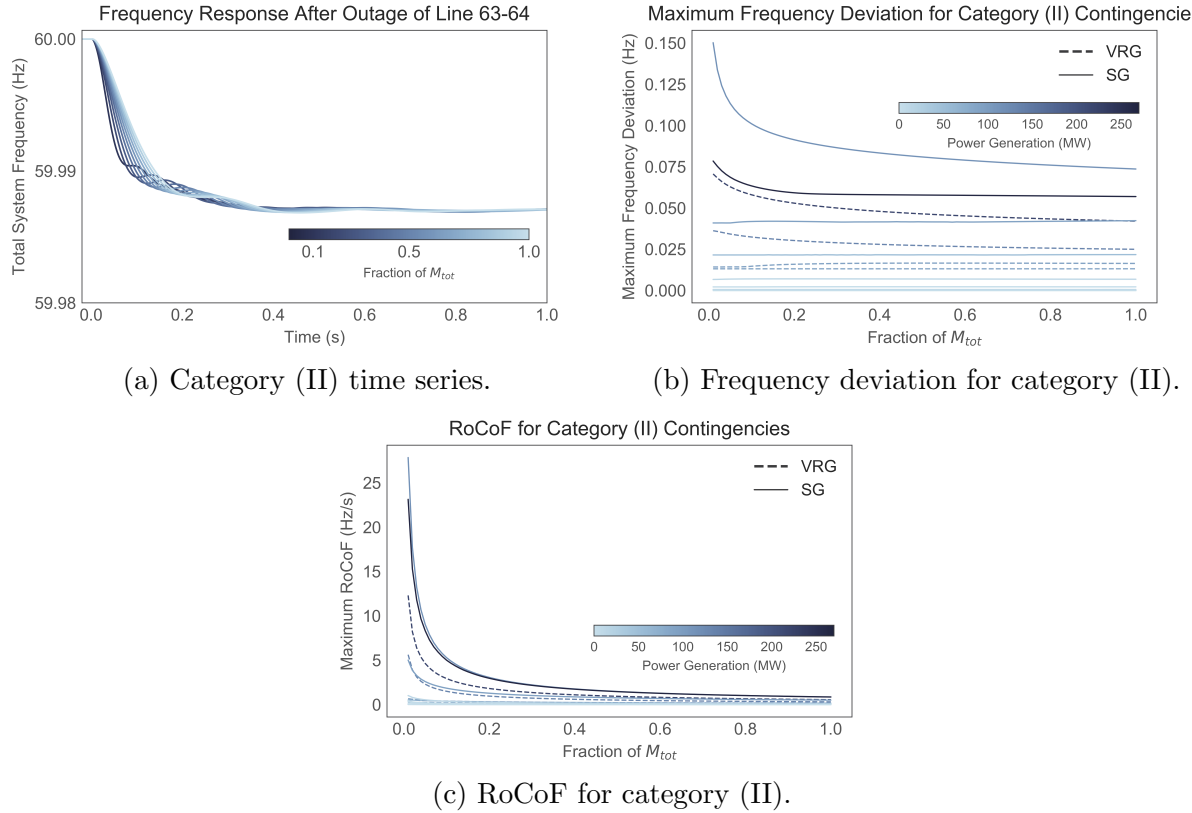


Figure 3.8: Category (II) time series and frequency dynamics.

different types of generation sources induces different dynamics. For example, Figure 3.8a shows the frequency time series at various inertia values after the removal of generator 64. Similar to the other categories the final settling value is unchanged based on total system inertia. Additionally, the RoCoF seems to increase as total system inertia decreases, which is seen for all these contingencies in Figure 3.8c. However, the first valley of the time series occurs at a lower frequency for higher values of total system inertia. This is opposite behavior from categories (I) and (III) (and category (IV) as discussed in a moment). Based on Figure 3.8b, there are only a few contingencies that actually decrease slightly as total system inertia decreases. Furthermore, two contingencies that start at the same maximum frequency deviation value for the base total system inertia have very different behavior as inertia is decreased. One possible reason this is occurring is based on the amount of power these generators are providing. Larger power providers, regardless of whether it is SG or

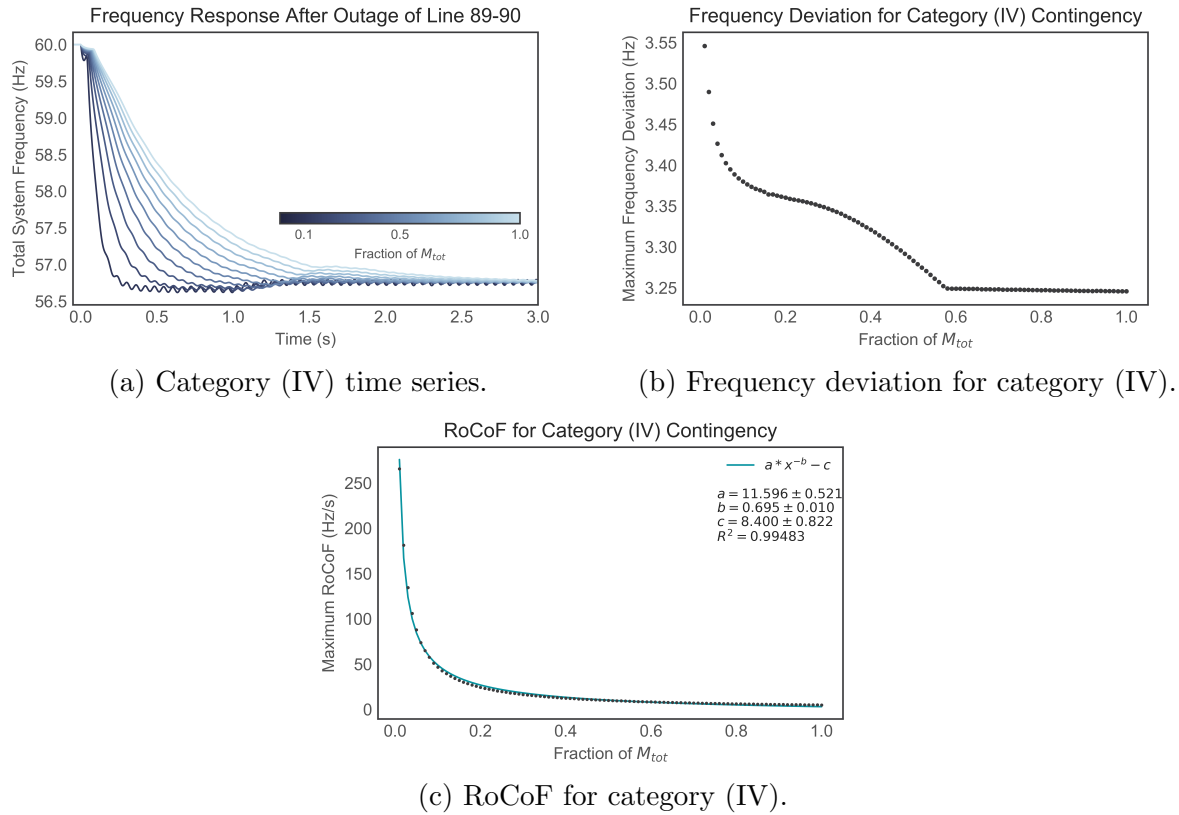


Figure 3.9: Category (IV) time series and frequency dynamics.

VRG, have a functional form similar to categories (I) and (III). This would explain the difference in the two contingencies that start at the same deviation at the base total system inertia, and then deviate. The second reason this could be occurring is illustrated by category (IV).

Figure 3.9 shows the dynamics for the category (IV) contingency of the Illinois test case. The time series has a similar step-like behavior as category (II), but it also has increased oscillatory behavior as inertia decreases like category (III). Furthermore, the RoCoF behavior is consistent with all other categories. However, the maximum frequency deviation has more complicated behavior. The deviation appears to change as a flat line until about 0.6 inertia where the concavity is inverted from the other plots, and then looks the same as the other ones at about $0.2M_{tot}$. Looking closely at Figure 3.9a, there are small oscillations for each inertia value, which grow in size as total system inertia decreases. Therefore, Figure 3.9b is

actually showing the exact point at which the oscillatory behavior “overcomes” the minimum fixed point value of ≈ 56.75 Hz. In the interval $0.01 - 0.2M_{tot}$ the maximum frequency deviation curve resembles that of other categories. This is a measurement in the growth in the oscillation amplitude after all other failures. For the loss of generation, the final “drop” is strictly a function of the amount of power lost. But, the occurrence of oscillatory behavior, as observed in Figure 3.9a is what determines if the curves in

To review, I broke up the cascading failure dynamics into four categories based on their outcomes. I then analyzed their trends from most stable to least and we found the following. First, although I took the total system inertia to extremely low values, it is incorrect to assume that the change in frequency deviation and RoCoF has a linear relationship with total system inertia. Second, the size of a frequency deviation is dependent on the network structure. In general, the frequency deviation size increases when a contingency is closer to large-inertia generation. However, even this has caveats: the substructure that the contingency is a part of probably determines its effects on stability. Finally, categories (II) and (IV) showed oscillatory behavior around the final frequency value that increased as total system inertia decreases.

Chapter 4

Conclusion

The preliminary results presented in Chapter 3 indicate the importance of inertia in power system dynamics during cascading failures. Specifically, I showed that the frequency dynamics have a non-linear dependence on total system inertia. By only using a limited range of inertia values, previous work had implicitly assumed a linear relationship [24][46]. This has implications for policy makers that will decide how to change frequency limits of power system devices, which in turn impacts grid resiliency [CITE]. Furthermore, I indicated how network topology is a crucial aspect of frequency stability. Specifically, I defined a new metric called the *average inertia distance* that calculates the distance between a contingency and inertia providing generation. The average inertia distance generally captures the relationship between contingency location and the frequency dynamics. However, I showed that there is still nuance in this metric; even contingencies with low average inertia distance can have low frequency deviation.

Future work will verify the trends of experiment one on the South Carolina test case. This will strengthen the generalization of the results. Although the impact of system topology was revealed by experiment one, this will be more thoroughly investigated by experiment two. Time permitting, both experiments one and two will be conducted on the Texas In-

terconnection test case. This is a 10,000 bus test case created in a similar manner to the other two. Finally, the procedures used to create the South Carolina, Illinois, and Texas test cases allows for randomness. This means that experiments one and two could be conducted on a large set of networks that have statistical similarities, but different topology. An experiment of this size would provide statistically rigorous and generalizable results about the relationship between power system inertia and dynamics.

Bibliography

- [1] Synchronization and transient stability in power networks and nonuniform kuramoto oscillators. *SIAM J. Control Optim.*, 50(3):1616–1642.
- [2] S. Abe, Y. Fukunaga, A. Isono, and B. Kondo. Power system voltage stability. *IEEE Transactions on Power Apparatus and Systems*, PAS-101(10):3830–3840, 1982.
- [3] Energy Information Administration. Annual energy outlook 2018. Technical report, 2-6-2018.
- [4] A. Arenas, A. Daz-Guilera, J. Kurths, Y. Moreno, and C. Zhou. Synchronization in complex networks. *Physics Reports*, 469(3):93 – 153, 2008.
- [5] A. B. Birchfield, Ti Xu, K. M. Gegner, K. S. Shetye, and T. J. Overbye. Grid structural characteristics as validation criteria for synthetic networks. *IEEE Transactions on Power Systems*, 32(4):3258–3265, jul 2017.
- [6] M. B. Cain, R. P. O'Neill, and A. Castillo. History of optimal power flow and formulations, paper 1. Technical report, FERC, 2012.
- [7] J. Chen, J. S. Thorp, and I. Dobson. Cascading dynamics and mitigation assessment in power system disturbances via a hidden failure model. *International Journal of Electrical Power and Energy Systems*, 27(4):318 – 326, 2005.
- [8] Congress. Energy policy act of 2005. *Pub.L. 109-58*, 2005.

- [9] C. L. DeMarco. A phase transition model for cascading network failure. *IEEE Control Systems*, 21(6):40–51, Dec 2001.
- [10] I. Dobson, B. A. Carreras, V. E. Lynch, and D. E. Newman. An initial model for complex dynamics in electric power system blackouts. In *Proceedings of the 34th Annual Hawaii International Conference on System Sciences*, pages 710–718, 2001.
- [11] V. Donde, V. Lopez, B. Lesieutre, A. Pinar, C. Yang, and J. Meza. Identification of severe multiple contingencies in electric power networks. In *Proceedings of the 37th Annual North American Power Symposium, 2005.*, pages 59–66, 2005.
- [12] F. Dörfler and F. Bullo. Kron reduction of graphs with applications to electrical networks. *IEEE Transactions on Circuits and Systems I: Regular Papers*, 60(1):150–163, Jan 2013.
- [13] S. Eftekharnejad, V. Vittal, G. T. Heydt, B. Keel, and J. Loehr. Impact of increased penetration of photovoltaic generation on power systems. *IEEE Transactions on Power Systems*, 28(2):893–901, 2013.
- [14] EPA. Sources of greenhouse gas emissions, 2016. <https://www.epa.gov/ghgemissions/sources-greenhouse-gas-emissions> [Accessed: 8-27-2018].
- [15] M. J. Eppstein and P. D. Hines. A random chemistry algorithm for identifying collections of multiple contingencies that initiate cascading failure. *IEEE Transactions on Power Systems*, 27(3):1698–1705, 2012.
- [16] ERCOT. Inertia: Basic concepts and impacts on the ERCOT grid, Apr 2018.
- [17] R. Fitzmaurice, E. Cotilla-Sanchez, and P. D. Hines. Evaluating the impact of modeling assumptions for cascading failure simulation. In *Power and Energy Society General Meeting, 2012 IEEE*, pages 1–8. IEEE, 2012.

- [18] P. D. Hines, I. Dobson, E. Cotilla-Sanchez, and M. Eppstein. “Dual Graph” and “Random Chemistry” methods for cascading failure analysis. In *2013 46th Hawaii International Conference on System Sciences*, pages 2141–2150, 2013.
- [19] P. Kundur, J. Paserba, V. Ajjarapu, G. Andersson, A. Bose, C. Canizares, N. Hatziargyriou, D. Hill, A. Stankovic, C. Taylor, T. Van Cutsem, and V. Vittal. Definition and classification of power system stability ieee/cigre joint task force on stability terms and definitions. *IEEE Transactions on Power Systems*, 19(3):1387–1401, 2004.
- [20] P. S. Kundur. *Power System Stability and Control*, pages 1–12. CRC Press, 2012.
- [21] Matthew Lave and Jan Kleissl. Solar variability of four sites across the state of colorado. *Renewable Energy*, 35(12):2867–2873, 2010.
- [22] H. Li, A. L. Bornsheuer, T. Xu, A. B. Birchfield, and T. J. Overbye. Load modeling in synthetic electric grids. In *2018 IEEE Texas Power and Energy Conference (TPEC)*, pages 1–6, Feb 2018.
- [23] F. Milano, F. Dörfler, G. Hug, D. Hill, and G. Verbic. Foundations and challenges of low-inertia systems. In *Power Systems Computation Conference (PSCC)*, Dublin, Ireland, 2018. To appear.
- [24] N. W. Miller, M. Shao, S. Pajic, and R. D’ aquila. Western wind and solar integration study phase 3 frequency response and transient stability. Technical report, National Renewable Energy Lab, Golden, CO, 2014.
- [25] D. P. Nedic, I. Dobson, D. S. Kirschen, B. A. Carreras, and V. E. Lynch. Criticality in a cascading failure blackout model. *International Journal of Electrical Power & Energy Systems*, 28(9):627 – 633, 2006.
- [26] NERC. A technical reference paper fault-induced delayed voltage recovery. 2009.

- [27] NERC. About nerc. <http://www.nerc.com/AboutNERC/Pages/default.aspx>, 7-11-2017.
- [28] NERC. Interconnections. <http://www.nerc.com/AboutNERC/keyplayers>, 7-11-2017.
- [29] T. Nishikawa and A. E. Motter. Comparative analysis of existing models for power-grid synchronization related content improving power grid transient stability by plug-in electric vehicles. *New Journal of Physics*, 17, 2015.
- [30] Electric Reliability Council of Texas. 2017 state of the grid, Apr 2018.
- [31] Australian Energy Market Operator. Black system south australia 28 september 2016 - final report, 2017.
- [32] Thomas J Overbye, Xu Cheng, and Yan Sun. A comparison of the ac and dc power flow models for lmp calculations. In *System Sciences, 2004. Proceedings of the 37th Annual Hawaii International Conference on*. IEEE, 2004.
- [33] Southwest Power Pool. Southwest power pool disturbance performance requirements, Jul 2016.
- [34] B. K. Poolla, S. Bolognani, and F. Dörfler. Optimal placement of virtual inertia in power grids. *IEEE Transactions on Automatic Control*, 62(12):6209–6220, December 2017.
- [35] K. Purchala, L. Meeus, D. Van Dommelen, and R. Belmans. Usefulness of dc power flow for active power flow analysis. In *Power Engineering Society General Meeting, 2005. IEEE*, pages 454–459. IEEE, 2005.
- [36] C. Roberts. Review of international grid codes, Feb 2018.
- [37] Peter W Sauer and MA Pai. Power system dynamics and stability. *Urbana*, 1998.

- [38] J. Song, E. Cotilla-Sanchez, G. Ghanavati, and P. D. Hines. Dynamic modeling of cascading failure in power systems. *IEEE Transactions on Power Systems*, 31(3):2085–2095, 2016.
- [39] Brian Stott, Jorge Jardim, and Ongun Alsaç. Dc power flow revisited. *IEEE Transactions on Power Systems*, 24(3):1290–1300, 2009.
- [40] A. Ulbig, T. S. Borsche, and G. Andersson. Impact of low rotational inertia on power system stability and operation. *IFAC Proceedings Volumes*, 47:7290–7297, 2014.
- [41] A. Von Meier. *Electric power systems: a conceptual introduction*. John Wiley & Sons, 2006.
- [42] Chengwei Wang, Celso Grebogi, and Murilo S Baptista. Control and prediction for blackouts caused by frequency collapse in smart grids. *Chaos: An Interdisciplinary Journal of Nonlinear Science*, 26(9):093119, 2016.
- [43] Yajun Wang, Horacio Silva-Saravia, and Hector Pulgar-Painemal. Estimating inertia distribution to enhance power system dynamics. pages 1–6, 2017.
- [44] T. Xu, A. B. Birchfield, and T. J. Overbye. Modeling, tuning, and validating system dynamics in synthetic electric grids. *IEEE Transactions on Power Systems*, 33(6):6501–6509, 2018.
- [45] T. Xu, A. B Birchfield, K. S Shetye, and T. J Overbye. Creation of synthetic electric grid models for transient stability studies. In *IREP Symposium Bulk Power System Dynamics and Control*, 2017.
- [46] T. Xu, Y. Liu, and T. J. Overbye. Metric development for evaluating inertia’s locational impacts on system primary frequency response. pages 1–6, Feb 2018.
- [47] T. Xu, Y. Liu, and T. J. Overbye. Metric development for evaluating inertia’s locational impacts on system primary frequency response. pages 1–6. IEEE, 2018.

- [48] Y. Yang and A. E. Motter. Cascading failures as continuous phase-space transitions. *Phys. Rev. Lett.*, 119(24):248–302, 2017.
- [49] R. D. Zimmerman, C. E. Murillo-Sánchez, and R. J. Thomas. Matpower: Steady-state operations, planning and analysis tools for power systems research and education. *Power Systems, IEEE Transactions*, 26:12–19, 2011.